**Authors response: We thank reviewer #2 for his valuable comments and for highlighting the importance of the work presented in this study in the context of the global carbon budget.**

**We addressed all comments raised by the reviewer and provide a point-by-point answer below (in blue). Changes and additions to the original manuscript have been introduced using the Word's "track changes" option and the line numbers noted in our answers refer to the revised manuscript with the track change option. We also took this opportunity to correct several typos in the manuscript.**

**On behalf of the co-authors,**
**Alizée Roobaert**

**Reviewer #2 Evaluations:**

Roobaert et al. assess the skill of the MOM6-COBALT model for representing the seasonal cycle of pCO2 in coastal regions and develop a methodology for interrogating the processes driving seasonal and regional differences. They use the model output to interrogate the drivers of the seasonal signal in three regions where model skill is high. This study makes good use of data products for assessing the skill of models in reproducing seasonal coastal dynamics and the unique information that models can bring to coastal carbon research, however, a few issues should be addressed before publication.

- **R2C1: 1) In the method to assess the different processes controlling seasonal pCO2 variability, the assumption that the coefficients (explained in lines 195-206) are constant in time needs to be explained.**

Are the coefficients truly constant in time if the goal is to understand how processes like freshwater discharge (a spring event in many regions) impact pCO2? Doesn't a spring-time river runoff event, for example, change the relationship between DIC, ALK, SSS, etc, which would not be reflected in coefficients derived from average conditions over 1998-2015?

**R2R1: We agree with the reviewer that residual biases between our regression-based reconstruction and the model $pCO_2$ can be attributed to strong seasonal signal in river discharge. The coefficients we use are indeed constant in time. We evaluated the impact of using coefficients that are both time and space varying and found that it further reduces biases tied to river discharge in the Amazon plume for instance. This improvement is, however, marginal compared to using the simpler approach we chose here (space-varying only). These residual biases are probably caused by the non-linearities associated with the large seasonal changes that the Takahashi linearization approach cannot capture even with time-varying coefficients. We agree with the reviewer that this is however an important point to make in the manuscript. We therefore added a panel to Figure S1 that shows the $pCO_2$ in the model and the $pCO_2$ reconstructed using the three different methods (traditional space varying coefficients from Sarmiento and Gruber, space varying regression method used here, and space and time varying regression method) at a point in the Amazon plume and added a paragraph to the method section that discusses this point which now reads as follows (lines 200-230):**

"In this study, we refine the estimation of the coefficients so they can be used for the wide range of DIC/ALK ratios that can be encountered in the coastal waters. This includes conditions when the DIC/ALK ratio is close to 1, such as in regions with significant freshwater discharge like those found near estuarine mouths or on polar shelves subject to sea-ice melting, when pH is around 7.5 (Egleston et al., 2010). In these cases, the traditional approximation method using mean DIC, ALK, SSS and SST fields breaks down (see Eq. (S1-S2) and Figure S1 in the Appendix). To circumvent this important limitation, we computed the coefficients of the $pCO_2$ dependency using a regression approach based on the CO2SYS program (Lewis and Wallace,

1998). At each point in space, $pCO_2$ was computed using the 1998 - 2015 average of DIC, ALK, SSS and SST with CO2SYS (method 14 in CO2SYS Matlab program, Millero, 2010). The $\frac{\partial pCO_2}{\partial DIC}$ coefficient was then computed as the slope of the linear regression between $pCO_2$ and DIC obtained by allowing DIC to vary around the local mean DIC value while keeping other tracers (ALK, SST, SSS) constant. The DIC range used to compute the slope was set to the ± 2 standard deviation of the 1998-2015 monthly values at that location with an upper bound at ± 60 µmol $kg^{-1}$ (see Appendix for further details). The same approach was repeated to compute the coefficients for the $pCO_2$ dependence on ALK, SST and SSS, respectively. Our methodology leads to coefficients that are constant in time but space dependent. In Fig. S1, we compare the coastal $pCO_2$ reconstructed from the traditional decomposition (using the space varying ~~empirical~~ coefficients reported by Sarmiento and Gruber, 2006) with those computed here using the CO2SYS regression. For the global coastal ocean, we find a large bias (global mean rmse of fitting $pCO_2$ anomaly in Eq. (2) = 14.6 µatm), which is especially pronounced at high latitudes. In contrast, the decomposition method based on our methodology reduce drastically the biases (global mean rmse = 2.8 µatm) in coastal regions and allows a more robust reconstruction of the $pCO_2$ variability.

We further evaluated how using coefficients that are both time and space varying could reduce the residual biases between our $pCO_2$ decomposition (using space dependent coefficients that are constant in time) and the $pCO_2$ simulated in the model that are found in regions with large freshwater discharge, such as the mouth of the Amazon River or Arctic coastal waters. We compare the $pCO_2$ seasonality simulated by the model to the $pCO_2$ reconstructed by the three methods (space varying coefficients from Sarmiento and Gruber (2006); regression-based space varying coefficients; and regression-based space and time varying coefficients) using a point in the Amazon River plume (points at 310.25°E - 1°N, Fig. S1d and S1e). At this location, the use of the regression-based coefficients greatly improves the recovery of the simulated $pCO_2$ compared to using the traditional coefficients of Sarmiento and Gruber (2006), reducing the rmse from 83 µatm to 24 µatm. The use of both space and time dependent regression-based coefficients further reduces this bias, bringing down the rmse from 24 uatm to 18 uatm. This additional improvement is however marginal, motivating our choice to use the simpler approach of the space dependent only coefficients."

## Updated figure S1:

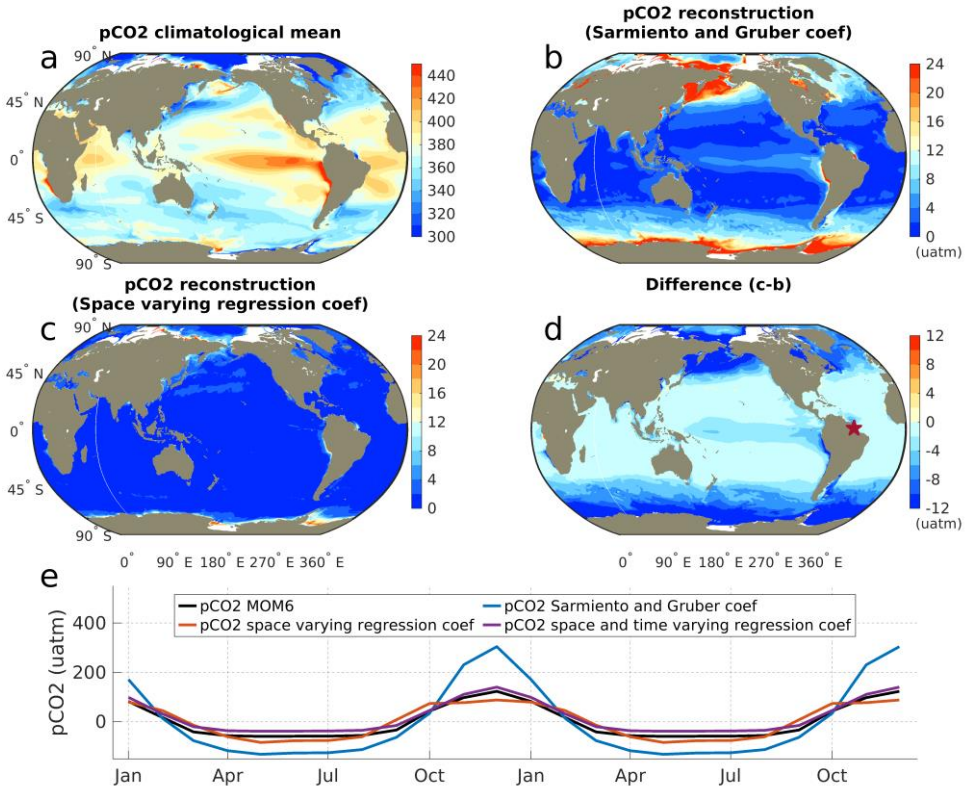


**Figure S1: Evaluation of ocean $pCO_2$ reconstruction methods using the same SST, SSS, DIC and ALK fields but different methods to derive the $pCO_2$ sensitivity coefficients ($\frac{\partial pCO_2}{\partial DIC}$, $\frac{\partial pCO_2}{\partial ALK}$, $\frac{\partial pCO_2}{\partial SST}$ and $\frac{\partial pCO_2}{\partial SSS}$): (a) ocean $pCO_2$ simulated by MOM6-COBALT, (b) bias in reconstructed $pCO_2$ using the approach widely used in the open ocean to compute sensitivity coefficients (Sarmiento and Gruber, 2006; Takahashi et al., 1993) and (c) bias in reconstructed $pCO_2$ using**

**the regression-based approach developed in this study to compute space varying sensitivity coefficients (using the CO2SYS program, see section 2.3 for details). (d) The difference in bias between the traditional and regression-based approaches shows a strong reduction in biases when using the regression-based method. Biases (in µatm) are quantified using the root mean square error (RMSE) between the $pCO_2$ simulated by the model and the $pCO_2$ reconstructed from simulated monthly SST, DIC, ALK and SSS (Eq. 2). (e) time series of seasonal $pCO_2$ anomaly at 310.25°E, 1°N (star on panel d) simulated by the MOM6 model (black), and reconstructed using the space varying coefficients of Sarmiento and Gruber 2006 (blue), using the space varying regression-based coefficients used in this study (red), and space and time varying regression-based coefficients (purple). See text in method section for further details.**

- **R2C2: 2)** In the methodological limitations section (3.1.4) it is mentioned the coastal-SOM-FFN climatology does have limitations in reproducing pCO2 variability in some regions. Since this is the case, for the regions where there are SOCATv6 data (lines 325-326 state there are 45 grids with sufficient data), **the paper should include model-SOCATv6 comparisons, especially for seasonal amplitude.**

Right now, Figure 4 does show SOCATv6 annual mean but Figure 5 does not show seasonal amplitude from SOCATv6, and seasonal amplitude is, as the authors state, underrepresented by coastal-SOM-FFN. Figures 4 and 5 should both include SOCATv6 as well as the residuals between model and SOCATv6 (for the regions where there is observational data). This is also an issue with the supplemental tables, where Table S1 presenting annual mean does include SOCATv6 but S2 presenting seasonal amplitude does not. The paper should include a more robust assessment of model-SOCATv6 seasonal amplitude comparisons, given seasonality, not annual mean, is the central focus of the study.

**R2R2: In this comment, the reviewer highlights that the $pCO_2$-based product is limited in poorly sampled regions and that a more direct comparison of the $pCO_2$ seasonality simulated by the model against the SOCATv6 database would be valuable. This idea is also echoed in several later comments from the reviewer regarding a suggestion to update Fig. 4 (R2C5), the addition of a seasonal evaluation based on 45 grid cells with continuous SOCATv6 data (R2C6) or the addition of seasonal $pCO_2$ cycles from SOCATv6 in Fig. 6 (R2R12).**

**We looked at $pCO_2$ measurements extracted from time-series at mooring stations that could provide validation datasets for our model. A recent literature review (Sutton et al., 2019) provides an extensive overview of these stations, but as illustrated on this map extracted from the NOAA website (https://www.ncei.noaa.gov/access/ocean-carbon-data-system/oceans/Moorings/ndp097.html) the vast majority of these stations fall outside of the geographic limits of our coastal domain and data collection at mooring stations in the coastal domain, such as along the north American coast only began, at the earliest (2004), mid-way through the time period represented by our study (1998-2015).**

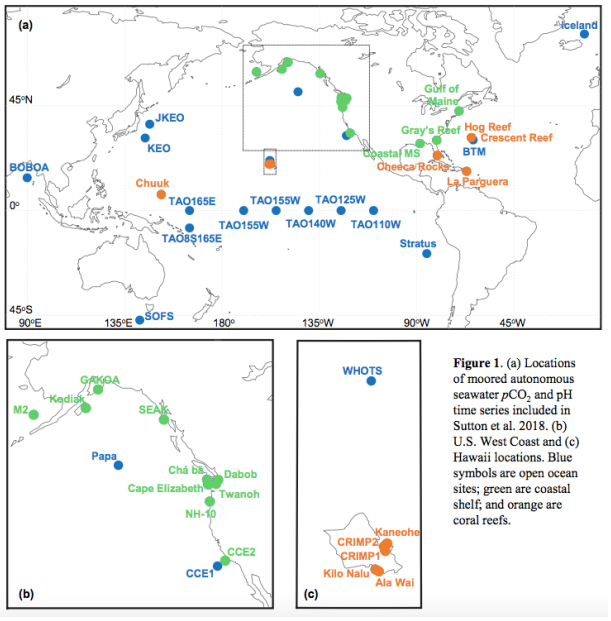


**Figure 1**. (a) Locations of moored autonomous seawater $pCO_2$ and pH time series included in Sutton et al. 2018. (b) U.S. West Coast and (c) Hawaii locations. Blue symbols are open ocean sites; green are coastal shelf; and orange are coral reefs.

**Figure from https://www.ncei.noaa.gov/access/ocean-carbon-data-system/oceans/Moorings/ndp097.html**

**Nevertheless, following the reviewer's suggestion we addressed the reviewer's concern by expanding our validation of the results using raw SOCATv6 data.**

**1) First, we updated our Fig. 6 and now present at the spatial resolution of 0.25 degree, the number of climatological months where at least one $pCO_2$ measurement is available based on the climatological seasonal cycle derived from the SOCATv6 database (new Fig. 6a). We believe this map provides valuable insight to the reader regarding both the spatial and temporal heterogeneity of the data coverage of the SOCATv6 database.**

**2) At the MARCATS scale, we selected 11 MARCATS with a good spatio-temporal coverage of the SOCATv6 database and for which is it possible to obtain a complete climatological seasonal cycle (see our new Fig. 6). The 11 MARCATS regions are the Californian Current (M2), Tropical E Pacific (M3), the Gulf of Mexico (M9), the East coast of US (M10), S Greenland (M15), Norwegian Basin (M16), NE Atlantic (M17), Iberian upwelling (M19), Moroccan upwelling (M22), China Sea and Kuroshio (M39) and New Zealand (M36). For each of these MARCATS, we calculated climatological seasonal $pCO_2$ cycles derived from the model, SOCATv6 and the coastal-SOM-FFN product (new Figs. 6b-l). For these regions, we calculated the bias between the seasonal amplitude of MOM6-COBALT and the one of SOCATv6 as well as their respective Pearson correlation coefficient. All these new values have been added to the updated Table S2 (see at the end of this document) in bracket to provide the reader with additional information regarding the model performance wherever there were enough field data to evaluate the model against Socatv6. Note that we did not perform the SOCATv6-model seasonal evaluation (bias and Pearson correlation coefficient) for the others MARCATS because of the lack of temporal coverage (new Fig. 6a). This is also the reason why we did not update Fig. 5 with a map of the seasonal $pCO_2$ amplitude from SOCATv6 as proposed by R2.**

**3) Finally, we selected 4 sites that are that are significantly smaller than the MARCATS scale and located in regions where the seasonal evaluation against SOCATv6 is not possible at the MARCATS scale. These sites are located off the Antarctic Peninsula, on the Queensland Plateau in NE Australia, in coastal waters of Papua New Guinea and of Terra Nova (see black boxes in new Fig. 6a). These sites present a complete seasonal climatological $pCO_2$ signal derived from SOCATv6 which can be compared to the model. The seasonal cycles for these four sites have been added to the updated Fig. 6 (panels m-p).**

## Updated Fig. 6:

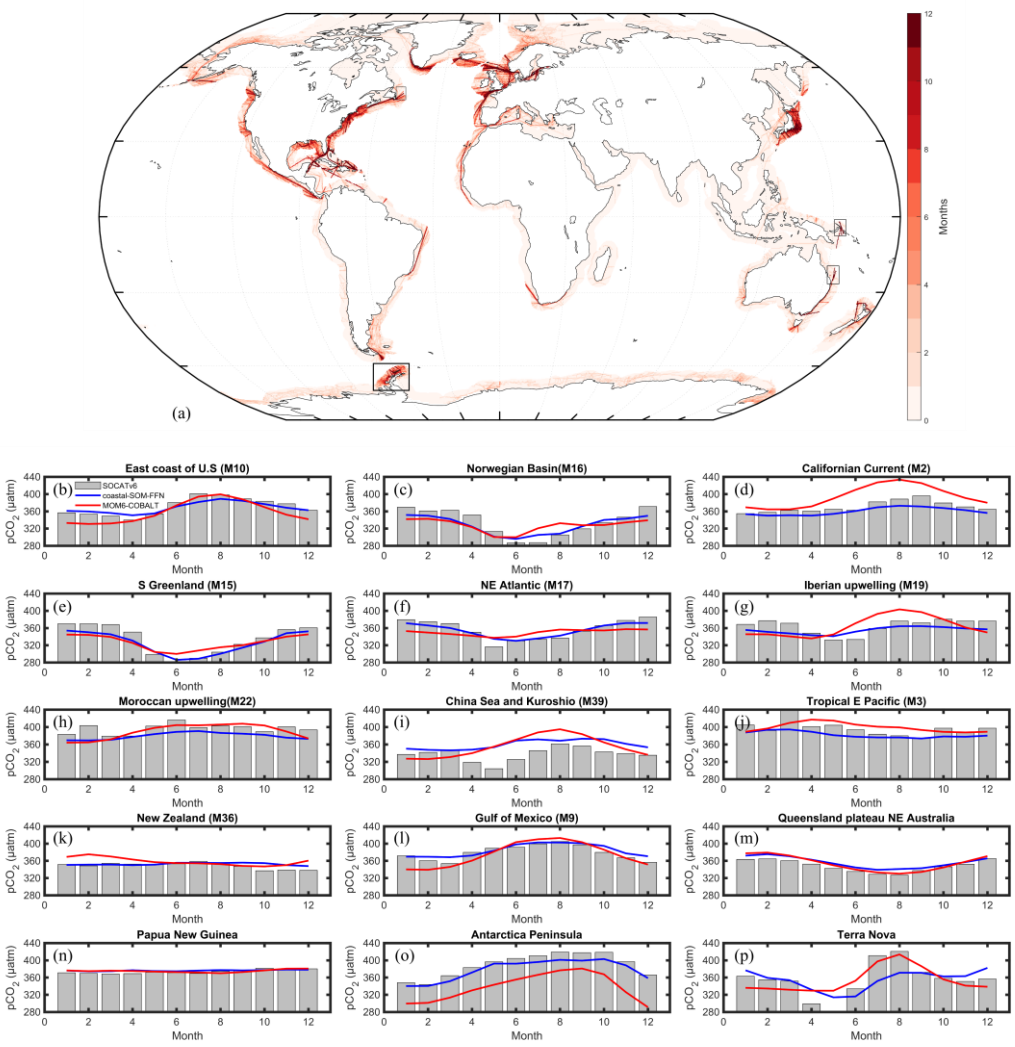


Figure 6: (a) SOCATv6 temporal coverage evaluated as the number of months (1 to 12) where at least one $pCO_2$ measurements is available (see details in methods). Seasonal $pCO_2$ cycle (µatm) derived from SOCATv6 (bar in grey), coastal-SOM-FFN (in blue), ~~and~~ and simulated by MOM6-COBALT (in red) for several MARCATS (b-l) and four coastal sites of smaller spatial extent than MARCATS (m-p). The location of the four coastal sites is represented in black boxes in panel (a). ~~(a) the East coast of the U.S (M10), (b) the Norwegian Basin (M16), (c) the West coast of North America (M2) and for (d) New Zealand (M36).~~ Month 1 corresponds to January. For consistency of y axis between panels, the value of 276 µatm is not represented in panel (p) for month 5 for the SOCATv6 data.

## Overall, as a consequence of this new evaluation strategy, Fig. 4 (see R5C5), Fig. 6, and Table S2 have been updated as well as the following sections of the manuscript:

## Lines 164-170:

"We use two metrics to evaluate SOCATv6 spatial and temporal coverage. First, we evaluate the spatial coverage at the MARCATS scale by computing the percent surface area sampled by SOCATv6 data for each MARCATS. A 50 % spatial coverage means that SOCATv6 data are available in 50 % of the 0.25° x 0.25° cells included in this specific MARCATS (this metric is used in Fig. 1a). Second, we evaluate the ability of SOCATv6 to capture the seasonality at the grid cell scale by computing the number of months where at least one SOCATv6 $pCO_2$ measurement for each 0.25° x 0.25° grid cells. A 8-months temporal coverage means that 8 out of the 12 months are sampled at least once in this grid cell (this metric is used in Fig. 6a)."

## lines 349-392:

"Our analysis reveals that the seasonal amplitudes simulated by MOM6-COBALT are systematically larger than the ones estimated by the coastal-SOM-FFN product (Fig. 5a-b, red colors in Fig. 5c and positive biases in Table S2) for all coastal regions belonging to EBC, WBC, Indian and tropical margins. For the majority of polar and subpolar margins and for some marginal seas, the model simulates lower seasonal $pCO_2$ amplitudes (blue colors in Fig. 5c and negative biases in Table S2). ~~Note that the seasonal evaluation is only performed against the coastal-SOM-FFN product because only few 0.25° coastal cells (approximately 45) in the Socatv6 database contain complete continuous $pCO_2$ time series.~~ Quantitatively, absolute biases between the modelled and coastal-SOM-FFN amplitudes do not exceed 20 µatm except for marginal seas where larger discrepancies are calculated (6 of the 9 marginal MARCATS, Table S2). The monthly mean $pCO_2$ seasonal cycle simulated by MOM6-COBALT is also well in phase (Pearson correlation coefficients > 0.5) with the one extracted from coastal-SOM-FFN in 34 out of the 45 MARCATS (red colors in Fig. 5d and Table S2). The agreement is especially good in the best monitored MARCATS regions (MARCATS where > 50 % of the area is covered by SOCATv6 observations, Table S1). For instance, in regions with good data coverage such as along the East coast of the U.S (M10), the Norwegian Basin (M16), the Californian Current (M2), the Leeuwin Current (M33), or the Brazilian Current (M6), the Pearson correlation coefficient is higher than 0.9 (Table S2). In contrast, the seasonal $pCO_2$ cycle simulated by MOM6-COBALT substantially diverges from that of the coastal-SOM-FFN in four poorly monitored marginal seas and in a few of the EBCs, Indian margins, subpolar margins, and tropical margins (Pearson correlation coefficient < 0.5, Table S2 and blue colors in Fig. 5d).~~.~~

The model $pCO_2$ seasonal evaluation against SOCATv6 is only performed in 11 MARCATS namely the Californian Current (M2), Tropical E Pacific (M3), the Gulf of Mexico (M9), the East coast of US (M10), S Greenland (M15), Norwegian Basin (M16), NE Atlantic (M17), Iberian Upwelling (M19), Moroccan upwelling (M22), China Sea and Kuroshio (M39) and New Zealand (M36). The modeled seasonal cycle is in good agreement with that one derived from SOCATv6 (Fig. 6b-n, Table S2) with absolute biases < 20 µatm for all of the 11 selected MARCATS and Pearson correlation coefficients close to 0.5 or higher except for the Iberian Upwelling (M19, Pearson value of 0.2) and in the New Zealand shelf (M36, value of 0.3). We did not perform the SOCATv6-model seasonal evaluation for the other MARCATS because the vast majority of grid cells only include data for less than 4 climatological months (Fig. 6a). However, ~~agreement is especially good in the best monitored MARCATS regions (MARCATS where > 50 % of the area is covered by Socatv6 observations, Table A1). For instance, in regions with good data coverage such as along the East coast of the U.S (M10, Fig. 6a), the Norwegian Basin (M16, Fig. 6b), the Californian Current (M2, Fig. 6c), the Leeuwin Current (M33), or the Brazilian Current (M6), the Pearson correlation coefficient is higher than 0.9 (Table A2). In contrast, the seasonal $pCO_2$ cycle simulated by MOM6-COBALT substantially diverges from that of the coastal-SOM-FFN in four poorly monitored marginal seas (M12, M21, M28, M29)~~ we also evaluated the simulated $pCO_2$ seasonality against SOCATv6 in regions where this evaluation is not possible to be performed at the MARCATS scale. To do so, we selected four~~-~~ sites of smaller spatial extent than MARCATS for which we calculated climatological seasonal $pCO_2$ signals from the SOCATv6 dataset and compared them with the model $pCO_2$. These sites are located off the Antarctic Peninsula, on the Queensland Plateau in NE Australia, in coastal waters of Papua New Guinea and of Terra Nova (see black boxes in Fig. 6a). In those regions, the absolute biases on the seasonal amplitude between MOM6-COBALT and SOCATv6 (Figs. 6m-p) are less than 20 µatm and the phase in the seasonal cycles present a good agreement with a Person correlation coefficient value of 0.8 except for the Papua New Guinea (value of 0.5). Note that the model-SOCATv6 seasonal evaluation in Terra Nova presents a good agreement although the MARCATS scale (Sea of Labrador, M11) evaluation to which this region belongs to reveals a low agreement, showing that a poor agreement between coastal-SOM-FFN and the model does not equate to poor model skill when these regions are under sampled by SOCATv6.

~~and in a few of the EBCs, Indian margins, subpolar margins (e.g., New Zealand, Fig. 6d) and tropical margins (Pearson correlation coefficient < 0.5, Table A2 and blue colors in Fig. 5d).~~"

## Lines 446-451:

"This lack of observations could partly explain why MOM6-COBALT-coastal-SOM-FFN $pCO_2$ biases exceed 20 µatm in these regions. ~~The seasonal model evaluation against raw SOCATv6 is limited at the MARCATS scale and mainly performed against coastal-SOM-FFN due to the very few coastal regions that contain a continuous climatological seasonal $pCO_2$ cycle (Fig. 6a) in the SOCATv6 database.~~ This study highlights the regions (Fig.1a, e.g., Indian ocean margins, Peruvian upwelling, marginal seas) where new observational data are most urgently needed, specifically collected ~~during periods of the years that are currently not covered~~ to improve our understanding of the $CO_2$ exchange between coastal regions and the atmosphere at the regional and global scales."

- **R2C3: 3) The ESRL atmospheric data are not properly cited.**

First, ESRL does not provide pCO2 as stated in line 115. The atmospheric community measures and provides xCO2. The authors need to properly cite the ESRL data source (not the current citation of Joos and Spahni) and explain how atmospheric pCO2 was calculated.

**R2R3: We thank the reviewer for drawing our attention to this issue in the original text. It should read $xCO_2$ instead of $pCO_2$ from ESRL. $xCO_2$ was converted to $pCO_2$ using atmospheric pressure and water vapor pressure by the model. The ESRL $xCO_2$ is from the NOAA Marine Boundary Layer (MBL) (https://gml.noaa.gov/ccgg/mbl/index.html). We modified the description and added the following two references.**

**Conway, T.J., P.P. Tans, L.S. Waterman, K.W. Thoning, D.R. Kitzis, K.A. Masarie, and N. Zhang, 1994, Evidence for interannual variability of the carbon cycle from the NOAA/CMDL global air sampling network, J. Geophys. Res., 99, 22831-22855.**

**GLOBALVIEW-CO2: Cooperative Atmospheric Data Integration Project - Carbon Dioxide. CD-ROM, NOAA ESRL, Boulder, Colorado [Also available on Internet via anonymous FTP to ftp.cmdl.noaa.gov, Path: ccg/co2/GLOBALVIEW], 2011. See version history (gml.noaa.gov/ccgg/globalview/co2/co2_version.html).**

**We modified the text lines 116-120:**

"The ocean model is forced by the 55-km horizontal resolution Japanese atmospheric reanalysis (JRA55-do) version 1.3 at a 3-hour frequency between 1959 and 2018 (Tsujino et al., 2018), and the atmospheric ~~p~~$CO_2$ concentration data ($xCO_2$) from the Earth System Research Laboratory ~~(Joos and Spahni, 2008)~~ (Conway et al., 1994; GLOBALVIEW-CO2, 2004). The $xCO_2$ is converted to $pCO_2$ using atmospheric and water vapor pressures by the model."

Minor issues:

- **R2C4: Line 45: This statement seems to be Northern Hemisphere biased.**

Given this study used a SOCAT-based data product, Southern Hemisphere coastal regions are extremely underrepresented and many areas are likely not well characterized.

**R2R4: The study by Roobaert et al. (2019) is indeed indirectly based on the SOCAT data product. However, we would like to stress out that we used the data product of Laruelle et al. (2017) which is a continuous $pCO_2$ climatology in space and time that fills out coastal regions devoid of data and underrepresented in the SOCAT database. This choice was motivated by the need to work with a $pCO_2$ field that included the entirety of the world's coastal ocean and would thus not be skewed by the current spatial heterogeneity of the SOCAT database. In their analysis of the $FCO_2$ seasonality, Roobaert et al. (2019) show a 6-month shift on the seasonal signal between "low" latitudes (40° N - 40° S) and high latitudes (> 60°). The latter latitudinal band has a more intense $CO_2$ sink occurring in summer both in the Northern and Southern hemispheres (see panels (a) and (d) in Fig. 5 of Roobaert et al. 2019). The more intense global coastal sink that occurs in summer that we associated only with the Northern Hemisphere, is in our view not a bias due to an under-representation of the southern hemisphere but only from the differing areal distribution of the coastal regions. Indeed, as shown by panel (c) of Fig. 4 of Roobaert et al., a large majority of the coastal surface lies in the high latitude of the Northern Hemisphere.**

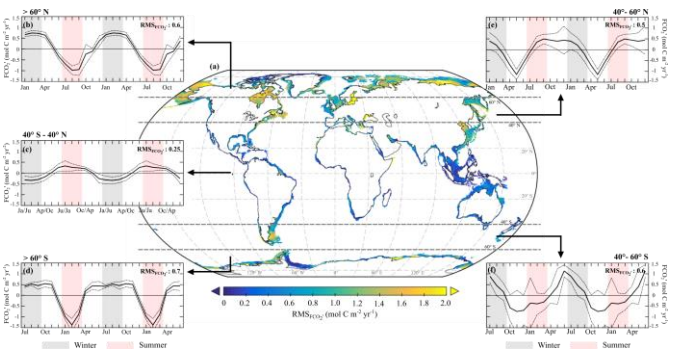

Fig. 5 of Roobaert et al. (2019)

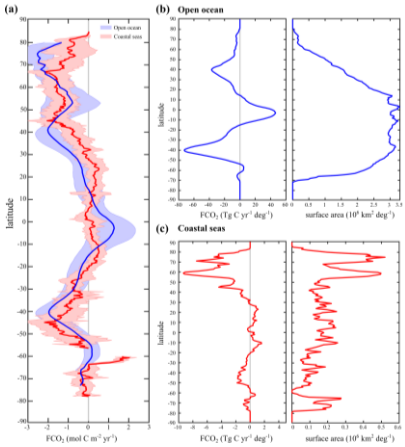

Fig. 4 of Roobaert et al. (2019)

**We believe that the phrasing of the following sentence (lines 43-48) in the manuscript might have led to a misunderstanding that we hope this updated version will prevent:**

"This study identified that at the annual timescale, the global coastal ocean acts as an atmospheric $CO_2$ sink (-0.2 ± 0.02 Pg C $yr^{-1}$) with a more intense $CO_2$ uptake occurring in boreal summer because of the disproportionate contribution of high latitude coastal regions in the Northern Hemisphere which cover 25 % of the total coastal area and are characterized by an intense $CO_2$ sink in summer. ~~This study identified that at the annual timescale, the global coastal ocean acts as an atmospheric $CO_2$ sink (-0.2 ± 0.02 Pg C $yr^{-1}$) with a more intense $CO_2$ uptake occurring in summer because of the disproportionate influence of high latitude coastal seas in the Northern Hemisphere.~~"

**R2C5: Line 290 / Figure 4: As stated earlier, it would be easier to see the model-data difference if a residual plot was included rather than ask the reader to compare Fig 4a and 4b.**

**R2R5: We agree with the reviewer's comment, which is directly connected to R2C2. We modified Fig. 4 and added a new panel (panel c) which represents the difference between the annual mean $pCO_2$ from MOM6-COBALT (Fig. 4a) and SOCATv6 (Fig. 4b). We also updated the text when we refer to this figure.**

**Updated Fig. 4**

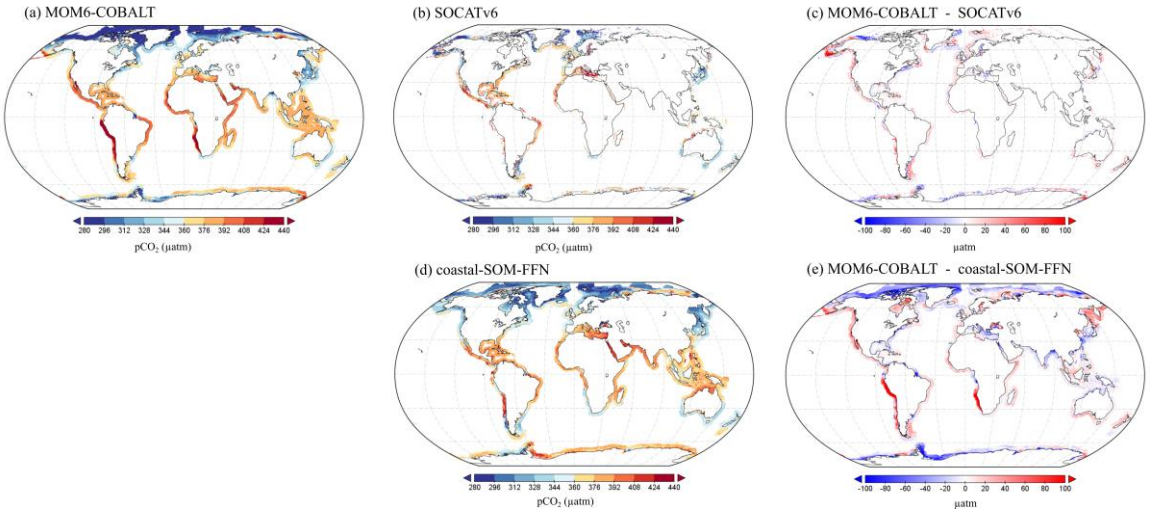


**Figure 4: Spatial distributions of the annual mean $pCO_2$ (µatm) generated by (a) MOM6-COBALT, (b) extracted from the SOCAT~~ocat~~v6 database, ~~and~~ (c) model bias as difference between panels (a) and (b) in µatm (red/blue colors correspond to regions in which the $pCO_2$ simulated by MOM6-COBALT is higher/lower than SOCATv6). (d) Spatial distribution of the annual mean $pCO_2$ from the coastal-SOM-FFN product (Laruelle et al., 2017). (~~e~~d) Model bias as**

**difference between panels (a) and (dc). ~~in µatm (red colors correspond to regions in which the $pCO_2$ simulated by MOM6-COBALT is higher than coastal-SOM-FFN).~~**

- **R2C6: Line 326: Many of these 45 grid cells with continuous pCO2 time series are likely buoy locations. Added to SOCAT in 2015, these continuous time series are an essential feature of SOCAT for seasonal assessments like this study and make a strong case for a more thorough model-data comparison as mentioned previously.**

**R2R6: We agree with the reviewer that a model-SOCATv6 seasonal analysis was missing in our original manuscript. We considered this comment and our new evaluation strategy regarding this issue is described in detail in the R2R2 response.**

- **R2C7: Line 352-353: In some places like here the regions are only stated by their associated numbers, however, it is easier for the reader to understand the results if stated by their name and number as in lines 356-357.**

**R2R7: We agree with R2C7 and modified some lines in the text accordingly.**

**Lines 316-320:** "The regions where the bias exceeds this threshold include two EBC's (the Californian (M2) and the Peruvian upwelling (M4) Currents), two marginal seas (the Seas of Japan, M40, and Okhotsk, M41), and one Polar (the Antarctic shelves, M45), subpolar (NW Pacific, M42) and Tropical East Atlantic (M23) shelf."

**lines 343-346:** "These regions belong mainly to EBCs (3 out of the 6 EBC MARCATS), marginal seas (3 out of the 9 marginal seas MARCATS), the remaining four being either polar (the Canadian Archipelago (M13) and the N Greenland ( M14)), subpolar (NW Pacific, M42) or Indian margins (the Bay of Bengal, M31)."

**lines 408-411:** "Note that these MARCATS but the Siberian (M43) and Antarctic~~,~~ (M45) shelves, the NE Pacific (M1), the Tropical E Atlantic (M23) and the Tropical W Indian (M26) also present an annual mean $pCO_2$ bias < 20 µatm in the MOM6-COBALT-~~Socatv6~~ SOCATv6 and coastal-SOM-FFN-~~Socatv6~~ SOCATv6 comparisons (Table S1)"

**Line 480:** "Interestingly however, some regions reveal significant biases in the major environmental fields but not in the $pCO_2$ (e.g., Tropical W Atlantic, M7) while in other regions, the reverse is observed (e.g., the Mediterranean (M20) and W Arabian ~~,~~(M27) Seas and in New Zealand (M36))."

- **R2C8: Lines 388-390: This seems to be an important result of the study that should be included in the Conclusion section."**

**R2R8: We agree with the reviewer's remark and introduced an explicit reference to this results in the updated version of the conclusion section in lines 595-600:**

"This study highlights the regions (Fig.1a, e.g., Indian ocean margins, Peruvian upwelling, marginal seas) where new observational data are most urgently needed, specifically data collected during different periods of the year that are currently missing to improve our understanding of the $CO_2$ exchange between coastal regions and the atmosphere at the regional and global scales."

- **R2C9: Section 3.2.1: Cai et al. 2020 find that different processes drive variation in pCO2 in different subregions of US East Coast. How do these model-based results compare with their data-based assessment of drivers?**

(See: Cai, W.-J., et al. (2020). Controls on surface water carbonate chemistry along North American ocean margins. Nature Communications, 11(1), 2691. https://doi.org/10.1038/s41467-020-16530-z)

**R2R9: We thank the reviewer for drawing our attention to this recent publication. The study of Cai et al. (2020) investigates the dynamics of the carbonate system along the continental margin of North America, thus including 2 of the MARCATS for which we provide a detailed analysis of the drivers controlling the seasonality of $pCO_2$ (the California current, M2, and the east coast of the US, M10). However, the work of Cai et al. mostly focusses on spatial variations and comparisons between the different coastal regions surrounding North America. In their study, the main references to the seasonal variability of $pCO_2$ (see page 9 in particular) focusses on the Atlantic coast of North America using a time-varying box model. In this region, the authors describe seasonal variations of $pCO_2$ similar to the ones reported in our study (with a $pCO_2$ increase from spring to summer and a decrease during fall leading to minimum $pCO_2$ values in winter). The brief description of the factors controlling these variations is also in line with the findings of our study with a thermally driven seasonality that is dampened by biological uptake. In the revised version of our manuscript, we now include 2 references to Cai et al.'s study in the section 3.2.1:**

**Line 515:** "This thermal effect was already identified by Signorini et al. (2013) in their observational study and further confirmed by ~~(~~Cai et al.~~,~~ ~~(~~2020)."

**Lines 540-542:** 'The importance of the thermal and circulation effects as well as the presence of a strong biological drawdown are in line with results from past studies (e.g., Laruelle et al. (2015), Shadwick et al. (2010, 2011), ~~and~~ Signorini et al. (2013) and ~~(~~Cai et al.~~,~~ ~~(~~2020~~)~~)."

- **R2C10: Lines 575-583: Description of the xCO2 data source is missing from this section.**

**R2R10: The source of the xCO2 data (i.e. Convey et al., 1994; GLOBALVIEW-CO2 project report) has now been introduced into the manuscript has requested by the reviewer.**

**We also added lines 645-647:** "The coastal-SOM-FFN $pCO_2$ datasets description and dataset can be downloaded from Laruelle et al. (2017) and the atmospheric $CO_2$ concentration data ($xCO_2$) derived from the Earth System Research Laboratory (Conway et al., 1994; GLOBALVIEW-CO2, 2004)."

**R2C11: Figure 3: This is another figure that could benefit from showing a MOM6-COBALT vs SOCATv6 comparison for pCO2.**

**R2R11: As stated in our answer to comment R2C5 which suggests that a map presenting the difference between the annual mean $pCO_2$ of MOM6-COBALT and that of SOCATv6 would be a valuable addition to Fig. 4, we find it difficult to add a panel comparing $pCO_2$ derived from SOCATv6 vs that one simulated by the model.**

**Indeed, all the panels in Fig. 3 display a comparison of the absolute values of different variables derived from observations versus those simulated by the model. This comparison is carried out at the MARCATS scale using continuous climatologies in space, i.e. each MARCATS is fully covered both in terms of observational data and by the model. Adding a panel comparing the absolute $pCO_2$ between SOCATv6 and MOM6-COBALT does not seem adequate given that the SOCAT data are spatially discontinuous. In addition, in several MARCATS, no data exist in the SOCATv6 database. The $pCO_2$ values derived from SOCATv6 would therefore not represent the mean value of MARCATS like those obtained in the $pCO_2$ coastal-SOM-FFN vs MOM6-COBALT comparison (panel f in Fig. 3). We did however significantly strengthen our model evaluation strategy (see detailed answer in R2C2) and believe we now provide substantially more material to the reader to be convinced of the ability of our model to adequately capture the seasonality of $pCO_2$.**

- **R2C12: Figure 6: If any of these regions have continuous pCO2 time series in SOCATv6, SOCATv6 should also be included.**

**R2R12: We agree with the comment. This is now part of our new strategy for the model evaluation as discussed in our response to R2R2. Figure 6 was updated accordingly.**

**Supplementary correction:**

**Color bar of panel (d) in Fig. 5 has been changed for a better visibility.**

**We also replaced "model skill" by "model to coastal-SOM-FFN agreement" in the manuscript to emphasize the fact that a low agreement does not equate a poor model skill in regions with low data density.**

**Updated Fig. 5**

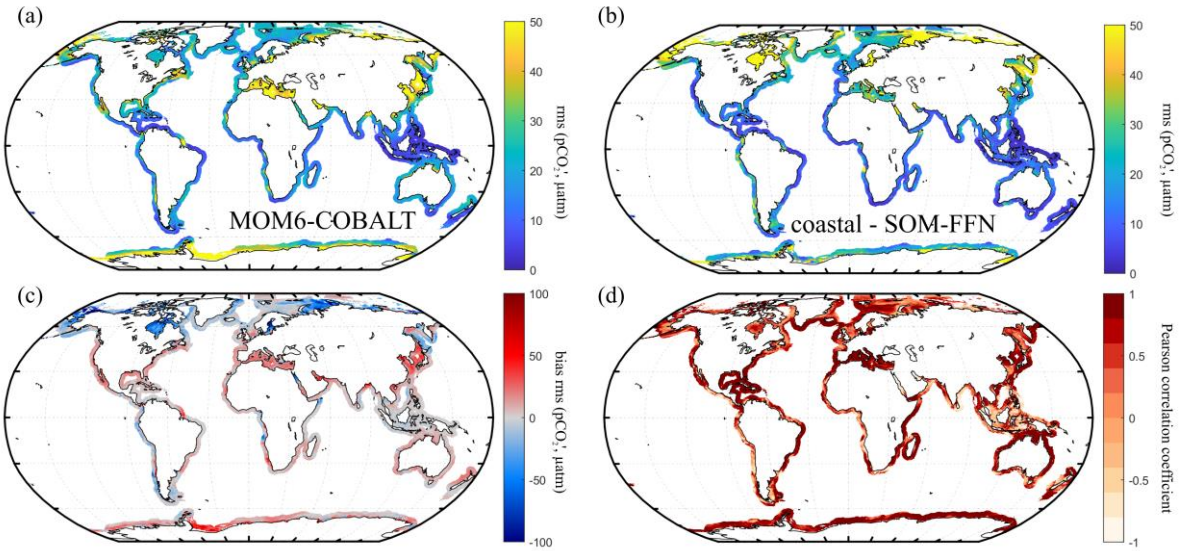

## Updated Table S2:

**Table S2: Seasonal evaluation of MOM6-COBALT against observations (SST, SSS, nutrients and $pCO_2$) for each MARCATS. The observational SST and SSS fields are from the NOAA OI SST V2 (Reynolds et al., 2007) and the EN4 SSS (Good et al., 2013). The observational nutrients derived from the World Ocean Atlas version 2018 (Garcia et al., 2019).The evaluation is performed on their seasonal amplitude which is expressed as the bias between the RMS of their amplitude. A positive value indicates higher values simulated by MOM6-COBALT compared to observations. The seasonal evaluation is also performed on their seasonal cycles which is represented by the Pearson correlation coefficient. A Pearson correlation coefficient value of 1 indicates that both signals are perfectly in phase with one another while a value of -1 represents a complete phase shift. Pearson correlation coefficient < 0.5 for $pCO_2$ are highlighted in red. The seasonal $pCO_2$ simulated by MOM6-COBALT is evaluated against coastal-SOM-FFN and for some MARCATS against SOCATv6 (in bracket).**

| MARCATS number (Mx) | MARCATS name | MARCATS category | Evaluation against data | | | | | | | | | | Evaluation against coastal-SOM-FFN (SOCATv6) | |
|---|---|---|---|---|---|---|---|---|---|---|---|---|---|---|
| | | | Bias RMS | | | | | Pearson correlation coefficient | | | | | Bias RMS | Pearson correlation coefficient |
| | | | SST (°C) | SSS (-) | Nutrients (µmol $kg^{-1}$) | | | SST | SSS | Nutrients | | | $pCO_2$ (µatm) | |
| | | | | | $NO_3$ | $PO_4$ | $SiO_4$ | | | $NO_3$ | $PO_4$ | $SiO_4$ | | |
| 2 | Californian Current | EBC | 0.0 | 0.0 | -0.1 | 0.0 | -0.4 | 1.0 | -0.3 | -0.2 | 0.2 | -0.1 | 16.2 (17.6) | 1.0 (0.9) |
| 4 | Peruvian upwelling Current | EBC | 0.1 | 0.0 | 0.0 | 0.0 | -0.2 | 1.0 | 0.8 | 0.7 | 0.7 | 0.8 | 6.6 | -0.4 |
| 19 | Iberian upwelling | EBC | -0.2 | 0.0 | -0.8 | 0.0 | -0.7 | 1.0 | 0.7 | 1.0 | 0.9 | 0.6 | 15.6 (9.3) | 0.8 (0.2) |
| 22 | Moroccan upwelling | EBC | -0.1 | 0.0 | -0.3 | 0.0 | -0.7 | 1.0 | 0.8 | 0.6 | 0.6 | -0.1 | 8.7 (7.7) | 0.9 (0.5) |
| 24 | SW Africa | EBC | 0.1 | 0.0 | -0.3 | -0.1 | -0.9 | 1.0 | 0.7 | 0.9 | 0.0 | -0.4 | 4.2 | 0.9 |
| 33 | Leeuwin Current | EBC | 0.0 | 0.0 | -0.1 | 0.0 | -0.1 | 1.0 | 1.0 | 0.2 | 0.0 | 0.0 | 12.7 | 0.9 |
| 27 | W Arabian Sea | Indian margins | -0.1 | 0.0 | -1.0 | -0.1 | -1.1 | 1.0 | 0.7 | 0.9 | 0.8 | 0.5 | 3.6 | 0.3 |
| 30 | E Arabian Sea | Indian margins | 0.0 | -0.1 | 0.1 | 0.0 | -0.9 | 1.0 | 0.9 | 0.7 | 0.2 | 0.0 | 6.2 | 0.7 |
| 31 | Bay of Bengal | Indian margins | 0.1 | 0.5 | 2.0 | -0.1 | -1.8 | 1.0 | 0.9 | 0.5 | 0.7 | -0.1 | 13.5 | -0.2 |
| 32 | Tropical E Indian | Indian margins | -0.1 | 0.0 | -0.1 | 0.0 | -0.9 | 1.0 | 0.8 | -0.7 | 0.0 | -0.5 | 5.4 | 0.9 |
| 9 | Gulf of Mexico | Marginal sea | -0.3 | 0.0 | -0.4 | -0.1 | -0.5 | 1.0 | 0.6 | 0.1 | 0.1 | -0.7 | 12.9 (10) | 1.0 (0.9) |
| 12 | Hudson Bay | Marginal sea | -0.2 | 0.0 | 0.9 | 0.0 | 0.9 | 1.0 | 0.1 | 0.0 | -0.4 | 0.6 | -46.4 | 0.4 |
| 18 | Baltic Sea | Marginal sea | -0.5 | -0.1 | -0.1 | 0.0 | -2.0 | 1.0 | 0.9 | 0.9 | 0.9 | 0.6 | -44.4 | 0.9 |
| 20 | Mediterranean Sea | Marginal sea | -0.1 | 0.0 | 0.1 | 0.0 | -0.2 | 1.0 | 0.6 | 0.7 | 0.5 | 0.0 | 20.6 | 1.0 |
| 21 | Black Sea | Marginal sea | -1.3 | 0.1 | 3.1 | 0.2 | 1.2 | 1.0 | 0.9 | 0.6 | 0.6 | 0.5 | -116.9 | -0.5 |
| 28 | Red Sea | Marginal sea | 0.0 | -0.2 | -0.1 | 0.0 | -0.3 | 1.0 | 0.2 | 0.4 | 0.5 | -0.1 | -0.4 | -0.9 |
| 29 | Persian Gulf | Marginal sea | -0.2 | 0.0 | 0.1 | 0.0 | -0.1 | 1.0 | 0.9 | 0.0 | 0.5 | 0.7 | 30.7 | -0.9 |
| 40 | Sea of Japan | Marginal sea | -0.6 | 0.0 | -1.3 | -0.1 | -3.0 | 1.0 | 1.0 | 0.9 | 1.0 | 0.6 | 28.0 | 0.9 |
| 41 | Sea of Okhotsk | Marginal sea | -0.4 | 0.1 | -1.1 | -0.1 | -6.2 | 1.0 | 0.9 | 1.0 | 0.9 | 1.0 | -6.5 | 0.7 |
| 13 | Canadian Archipelago | Polar | -0.4 | 0.0 | 0.6 | 0.0 | -0.9 | 1.0 | 0.8 | 0.9 | 0.7 | 0.9 | -18.0 | 0.9 |
| 14 | N Greenland | Polar | 0.2 | 0.1 | -0.3 | 0.0 | -0.6 | 1.0 | 0.8 | 1.0 | 0.9 | 0.8 | -9.0 | 0.8 |
| 15 | S Greenland | Polar | 0.1 | 0.0 | 0.1 | 0.0 | -1.0 | 1.0 | 0.6 | 1.0 | 1.0 | 0.9 | -8.5 (-8.8) | 1.0 (1.0) |
| 16 | Norwegian Basin | Polar | 0.0 | 0.0 | -0.5 | 0.0 | -0.4 | 1.0 | 0.9 | 1.0 | 1.0 | 0.9 | -6.1 (-4.1) | 0.9 (0.7) |

| | | | | | | | | | | | | | | |
|---|---|---|---|---|---|---|---|---|---|---|---|---|---|---|
| 43 | Siberian Shelves | Polar | -0.4 | -0.4 | 0.9 | -0.1 | -4.0 | 1.0 | 0.6 | 0.5 | 0.4 | 0.6 | -15.7 | 0.9 |
| 44 | Barents and Kara seas | Polar | -0.2 | -0.3 | 0.1 | 0.0 | -1.1 | 1.0 | 0.6 | 0.9 | 0.9 | 0.6 | -7.4 | 0.7 |
| 45 | Antarctic Shelves | Polar | 0.2 | 0.1 | 2.0 | 0.1 | 1.3 | 1.0 | 0.9 | 1.0 | 0.9 | 0.6 | 13.3 | 1.0 |
| 1 | N-E Pacific | Subpolar | -0.1 | -0.1 | -1.2 | -0.2 | -5.6 | 1.0 | 0.9 | 0.9 | 0.9 | 0.8 | -4.5 | 0.8 |
| 5 | Southern America | Subpolar | -0.1 | 0.0 | -1.4 | -0.1 | -0.3 | 1.0 | 0.9 | 0.9 | 0.9 | 0.7 | -6.4 | 0.8 |
| 11 | Sea of Labrador | Subpolar | -0.2 | -0.1 | 0.3 | 0.0 | -0.5 | 1.0 | 1.0 | 0.9 | 0.9 | 0.9 | 0.8 | 0.2 |
| 17 | NE Atlantic | Subpolar | 0.0 | 0.1 | -0.8 | 0.0 | -0.7 | 1.0 | 1.0 | 1.0 | 1.0 | 1.0 | -8.2 (-12.5) | 0.6 (0.6) |
| 34 | S Australia | Subpolar | 0.2 | 0.0 | 0.3 | 0.0 | -0.2 | 1.0 | 0.6 | 0.9 | 0.7 | 0.2 | 12.8 | 0.9 |
| 36 | New Zealand | Subpolar | 0.0 | 0.0 | 0.4 | 0.0 | -0.3 | 1.0 | 0.7 | 0.8 | 0.8 | 0.6 | 6.2 (2.8) | -0.5 (0.3) |
| 42 | NW Pacific | Subpolar | -0.2 | 0.0 | -2.6 | -0.3 | -6.7 | 1.0 | 1.0 | 1.0 | 1.0 | 0.9 | -19.2 | 1.0 |
| 3 | Tropical E Pacific | Tropical | 0.0 | 0.0 | -0.5 | 0.0 | -1.3 | 0.9 | 1.0 | 0.0 | -0.4 | 0.3 | 3.1 (-3.3) | 0.3 (0.4) |
| 7 | Tropical W Atlantic | Tropical | 0.0 | 0.6 | 0.5 | -0.1 | -1.8 | 0.9 | 0.9 | 0.4 | 0.0 | -0.4 | 9.6 | 1.0 |
| 8 | Caribbean Sea | Tropical | -0.1 | 0.0 | -0.2 | 0.0 | -0.8 | 1.0 | 1.0 | -0.2 | -0.2 | -0.8 | 2.2 | 1.0 |
| 23 | Tropical E Atlantic | Tropical | -0.1 | 0.2 | -0.5 | 0.0 | -0.5 | 1.0 | 1.0 | 0.6 | 0.8 | -0.5 | 1.5 | 0.6 |
| 26 | Tropical W Indian | Tropical | 0.0 | 0.1 | 0.0 | 0.0 | -0.7 | 1.0 | 1.0 | -0.6 | 0.5 | 0.3 | 5.6 | 0.9 |
| 37 | N Australia | Tropical | 0.0 | 0.0 | 0.0 | 0.0 | -0.2 | 1.0 | 1.0 | 0.6 | 0.2 | 0.7 | 5.2 | 1.0 |
| 38 | SE Asia | Tropical | -0.2 | 0.1 | 0.0 | 0.0 | -1.0 | 1.0 | 1.0 | -0.2 | -0.3 | -0.1 | 8.9 | 0.2 |
| 6 | Brazilian Current | WBC | -0.1 | 0.0 | -0.5 | -0.1 | -0.9 | 1.0 | -0.2 | 0.8 | 0.7 | -0.4 | 7.5 | 0.9 |
| 10 | East coast of US | WBC | -0.5 | 0.0 | 0.0 | 0.0 | -0.3 | 1.0 | 1.0 | 0.9 | 0.9 | 0.8 | 12.4 (5.7) | 0.9 (0.9) |
| 25 | Agulhas Current | WBC | 0.0 | 0.1 | -0.1 | 0.0 | -1.0 | 1.0 | 1.0 | 0.4 | 0.1 | 0.3 | 8.1 | 1.0 |
| 35 | E Australian Current | WBC | 0.2 | 0.0 | 0.1 | 0.0 | -0.3 | 1.0 | 0.6 | 1.0 | 0.9 | 0.6 | 7.4 | 1.0 |
| 39 | China Sea and Kuroshio | WBC | -0.2 | 0.0 | -0.6 | 0.0 | -1.3 | 1.0 | 0.9 | 1.0 | 0.9 | 0.9 | 13.2 (9.1) | 0.9 (0.4) |

**Reference**


Cai, W.-J., Xu, Y.-Y., Feely, R. A., Wanninkhof, R., Jönsson, B., Alin, S. R., et al. (2020). Controls on surface water carbonate chemistry along North American ocean margins. *Nature Communications*, *11*(1), 1–13. https://doi.org/https://doi.org/10.1038/s41467-020-16530-z

Conway, T. J., Tans, P. P., Waterman, L. S., Thoning, K. W., Kitzis, D. R., Masarie, K. A., & Zhang, N. (1994). Evidence for interannual variability of the carbon cycle from the National Oceanic and Atmospheric Administration/Climate Monitoring and Diagnostics Laboratory Global Air Sampling Network. *Journal of Geophysical Research*, *99*(D11), 22831–22855. https://doi.org/10.1029/94jd01951

Egleston, E. S., Sabine, C. L., & Morel, F. M. M. (2010). Revelle revisited: Buffer factors that quantify the response of ocean chemistry to changes in DIC and alkalinity. *Global Biogeochemical Cycles*, *24*(1). https://doi.org/10.1029/2008GB003407

Garcia, H. E., Weathers, K. W., Paver, C. R., Smolyar, I., Boyer, T. P., Locarnini, R. A., et al. (2019). *NOAA Atlas World Ocean Atlas 2018. Vol. 4: Dissolved Inorganic Nutrients (phosphate, nitrate and nitrate+nitrite, silicate)*.

GLOBALVIEW-CO2. (2004). GLOBALVIEW-CO2: Cooperative Atmospheric Data Integration Project - Carbon Dioxide. *CD-ROM, NOAA/CMDL*.

Good, S. A., Martin, M. J., & Rayner, N. A. (2013). EN4: Quality controlled ocean temperature and salinity profiles and monthly objective analyses with uncertainty estimates. *Journal of Geophysical Research: Oceans*, *118*(12), 6704–6716. https://doi.org/10.1002/2013JC009067

Lewis, E. R., & Wallace, D. W. R. (1998). *Program developed for CO2 system calculations*. *Ornl/Cdiac-105*. Environmental System Science Data Infrastructure for a Virtual Ecosystem.

Millero, F. J. (2010). Carbonate constants for estuarine waters. *Marine and Freshwater Research*, *61*(2), 139–142. https://doi.org/10.1071/MF09254

Reynolds, R. W., Smith, T. M., Liu, C., Chelton, D. B., Casey, K. S., & Schlax, M. G. (2007). Daily high-resolution-blended analyses for sea surface temperature. *Journal of Climate*, *20*(22), 5473–5496. https://doi.org/10.1175/2007JCLI1824.1

Roobaert, A., Laruelle, G. G., Landschützer, P., Gruber, N., Chou, L., & Regnier, P. (2019). The Spatiotemporal Dynamics of the Sources and Sinks of CO2 in the Global Coastal Ocean. *Global Biogeochemical Cycles*. https://doi.org/10.1029/2019GB006239

Sutton, A. J., Feely, R. A., Maenner-Jones, S., Musielwicz, S., Osborne, J., Dietrich, C., et al. (2019). Autonomous seawater pCO2 and pH time series from 40 surface buoys and the emergence of anthropogenic trends. *Earth System Science Data*, *11*(1), 421–439. https://doi.org/10.5194/essd-11-421-2019

Tsujino, H., Urakawa, S., Nakano, H., Small, R. J., Kim, W. M., Yeager, S. G., et al. (2018). JRA-55 based surface dataset for driving ocean–sea-ice models (JRA55-do). *Ocean Modelling*, *130*, 79–139. https://doi.org/10.1016/j.ocemod.2018.07.002